Heliyon 10 (2024) e28097

Contents lists available at ScienceDirect

Heliyon

journal homepage: www.cell.com/heliyon

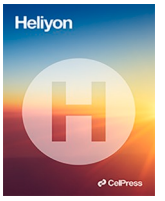

Research article

Composite polymer electrolyte based on poly(vinylidene fluoride-hexafluoropropylene) (PVDF-HFP) for solid-state batteries

Zhongran Yao [a], Fen Qi [b,*], Lin Ye [a], Qiang Sun [a], Xiaoyong Gu [a], Xiaowei Yang [a], Kongjun Zhu [c]

[a] School of Automobile and Transportation, Wuxi Institute of Technology, Wuxi, 214121, China
[b] Kai Yuan School of Innovation and Entrepreneurship, Wuxi Institute of Technology, Wuxi, 214121, China
[c] College of Aerospace Engineering, Nanjing University of Aeronautics and Astronautics, Nanjing, 210016, China

ARTICLE INFO

Keywords:
Solid-state electrolytes
Lithium-ion batteries
Composite polymer electrolyte
Electrochemical performance

ABSTRACT

Using solid-state electrolytes (SSEs) with excellent thermal and electrical stability to replace liquid electrolytes, and assembling solid-state lithium-ion batteries (SSLIBs) is considered the best solution to these safety issues. However, it is difficult for a single electrolyte to have the characteristics of high ionic conductivity, low interface resistance, and high stability of the counter electrode at the same time. In this work, the composite polymer electrolyte membrane (CPE) of inorganic $Li_{1.3}Al_{0.3}Ti_{1.7}(PO_4)_3$ (LATP) and organic poly(vinylidene fluoride-hexafluoropropylene) (PVDF-HFP) polymer was successfully prepared by traditional casting method. The addition of LATP (10 wt %) ceramic powder makes CPE membrane (CPE-10) exhibit excellent electrochemical performance: the lithium-ion transference number and electrochemical window are as high as 0.60 and 4.94 V, respectively. Moreover, the CPE-10 showed excellent Li-metal stability, thereby enabling the Li–Li symmetric cells to stably run for over 300 h at 0.1 mA/cm^2 with effective lithium dendrite inhibition. When paired with a high-voltage $LiNi_{0.6}Co_{0.2}Mn_{0.2}O_2$ (NCM622) cathode, the Li/CPE-10/NCM622 cell exhibited excellent electrochemical performance: the highest specific discharge capacity of 152 mAh/g could be conducted at 0.2C after 50 cycles corresponding to 100% Coulombic efficiencies. The prepared CPE-10 demonstrates excellent electrochemical performance, providing an effective design strategy for SSLMBs.

1. Introduction

Developing clean and efficient energy storage equipment is an effective strategy to solve the increasingly serious energy crisis and environmental pollution problems. Among various energy storage devices, lithium-ion batteries have become one of the most popular ones due to their large size and high energy density [1–3]. At present, the energy density of lithium-ion batteries based on intercalated materials is not only difficult to meet the requirements of long-distance transportation, but flammable liquid electrolytes also pose potential safety issues for batteries, especially in the application of large batteries in electric vehicles and power grids [4,5]. Solid-state lithium batteries using solid-state electrolytes have advantages such as higher energy density, longer cycle life, and better safety,

* Corresponding author.
E-mail address: qfwxit@163.com (F. Qi).

https://doi.org/10.1016/j.heliyon.2024.e28097
Received 4 January 2024; Received in revised form 9 March 2024; Accepted 12 March 2024
Available online 16 March 2024

making them an important research direction in the field of next-generation batteries [6–8].

Solid polymer electrolytes (SPEs), as a high-performance solid-state electrolyte system, have attracted widespread attention due to their excellent flexibility, wide operating temperature range, and excellent cycle life [8–11]. Meanwhile, SPEs can effectively inhibit the growth of lithium dendrites, thereby avoiding the occurrence of battery short circuits. With the continuous research and development of polymer electrolytes, various polymers have been widely studied, including polyethylene oxide (PEO) [12], polyvinylidene fluoride (PVDF) [9,13], PVDF-HFP [14–17], polyacrylonitrile (PAN) [18], polymethyl methacrylate (PMMA) [19], etc. As one of these candidates, PVDF-HFP has gained considerable interest as an electrolyte for energy storage devices due to properties like low crystallinity, high polarity, low crystallinity, high dielectric constant, affinity to the electrolyte, wide voltage window, significant adhesion to the electrode and presence of polar group (-C-F-) [14,20]. Nevertheless, the extensive application still impedes the solid polymer electrolyte applications are low ionic conductivity at ambient temperature and low transference number. To solve this problem, ceramic particles such as inert materials (TiO_2 [21]、SiO_2 [22]) or active materials (LLZO [23]、LATP [24,25]) are dispersed or embedded into the polymer matrix to construct organic-inorganic composite polymer electrolytes (CPEs), which can not only improve mechanical strength, but also reduce polymer crystallization, thereby enhancing ion migration [26,27]. Among the explored additives, NASICON type $Li_{1.3}Al_{0.3}Ti_{1.7}(PO_4)_3$ (LATP) ceramic electrolytes showed excellent thermal performance, air stability, and a remarkable enhancement of conductivity ($>10^{-4}$ S/cm) in comparison to compounds with similar crystal framework [28–30]. Y. J. Wang et al. demonstrated that the advantage of LATP as a filler is not only by generating an intense reduction of crystallinity and more flexible local chains in the amorphous phase, but also by possible dissolution and complexation with PEO [31].

Based on this, we report a composite solid electrolyte (CPE-10) based on PVDF-HFP polymer and LATP ceramic powder. The composite polymer electrolyte has advantages such as high ion conductivity, wide electrochemical window, high ion migration number, and high thermal stability. In addition, the NCM622 or $LiFePO_4$/CPE-10/Li solid-state lithium metal battery system were successfully assembled by matching it with the NCM622 and $LiFePO_4$ positive electrode, demonstrating excellent electrochemical performance.

2. Experimental

2.1. Materials synthesis

LATP power was synthesized by a modified co-precipitation method, described in detail in our previous work [32]. The LATP-modified PVDF-HFP composite electrolyte film (PVDF-HFP-*x* wt% LATP, abbreviated as CPE-*x*) was prepared by tape-casting method, where *x* represents the mass percentage of LATP ceramic powder in the composite polymer electrolyte. The specific preparation process is shown in Fig. 1. LATP particles and LiTFSI (99.95%, Macklin) with different weight percentages (0–35 wt %) were added to PVDF-HFP (Arkema, France, Kynar Flex 2801), and were continuously magnetically stirred in N, N-dimethylformamide (DMF) solution for 24 h. Then the formed uniform slurry is spread on the glass plate with a scraper and dried in a 60 °C vacuum oven to form a uniform polymer film.

2.2. Structural characterization

The phase structure of samples was collected on X-ray diffraction (XRD, Bruker D8) using Cu Kα radiation (λ = 1.5406 Å). Scanning electron microscopy (SEM, Hitachi S-4800, Japan) was applied to investigate the surface and cross-section morphologies of the polymer electrolytes and Li anode. The thin film electrolyte was quenched with liquid nitrogen to observe the characteristics of the electrolyte section. Fourier transforms infrared spectroscopy (FTIR, Nicollet NEXUS670, America) was recorded to determine the possible chemical reaction between the LATP phase and the polymer matrix. The test range was 4000~650 cm^{-1}. Simultaneous thermal analysis (TG-DSC, STA449F5 Jupiter, Netzsch, Germany) was used to analyze the sintering shrinkages of the film samples with temperature change at 5 °C/min in an N_2 environment.

2.3. Electrochemical tests

Electrochemical impedance spectroscopy (EIS) was carried out to test the ionic conductivity (σ) of the electrolyte from 10^{-1}

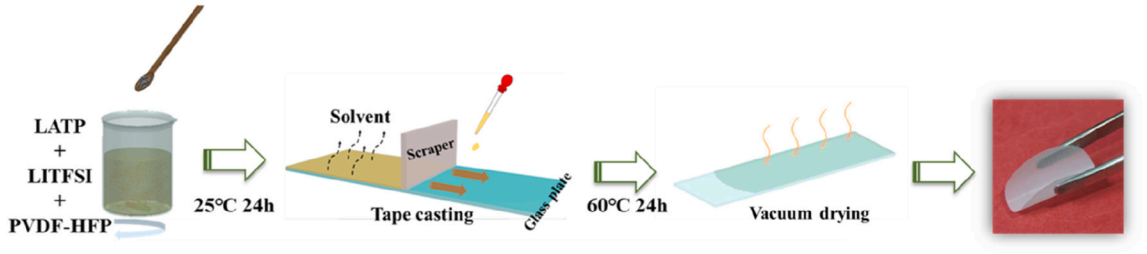

Fig. 1. Schematic of the fabrication process of CPE-10.

Hz–10^6 Hz. The σ was measured by EIS using a CHI660E electrochemical workstation and calculated by the formula: $\sigma = L/R \times S$, where S, L, and R, are the area of the composite electrolyte, membrane thickness and resistance measured by EIS, respectively. The ionic conductivity values corresponding to different temperatures are obtained, and the activation energy (E_a) values are calculated from this. The specific calculation formula involved in representing the relationship between E_a and the total impedance σ_t is (Arrhenius): $\sigma_t = Aexp(-E_a/k_BT)$, where k_B is the Boltzmann constant, A and T are the given parameters and the ambient temperature, respectively.

The lithium transference number (t_{Li+}) was calculated by the following equation: $t_{Li+} = I_{ss}(\Delta V - R_0I_0)/I_0(\Delta V - R_{ss}I_{ss})$, where ΔV is 10 mV DC polarization potential, I_0 and I_{ss} are initial and steady-state current respectively, R_0 and R_s are initial and steady-state resistance before and after AC polarization. Linear Sweep Voltammetry (LSV) is used to investigate the electrochemical window for the polymer electrolyte with SS/CPE/Li cells. The scanning rate is 10 mV/s and the electrochemical window is detected in the range of 1–6.0 V (vs Li+/Li) using an electrochemical workstation (CHI660E, Shanghai Chenhua Instrument Co., Ltd.)

It uses commercial 2032-type coin cells and consists of a composite positive electrode of 80 wt% $LiFePO_4$/NCM622 positive powder, 10 wt% PVDF–LiTFSI adhesive and 10 wt% Super-P. Subsequently, the composite positive electrode is added to N-methyl-pyrrolidone (NMP) solvent to obtain a thick paste, which is then coated on Al foil and dried overnight under a vacuum of 80 °C. The active material load was controlled to 2–3 mg/cm^2. The entire battery assembly process is carried out in an AR-filled glove box. In addition, to reduce the interface contact between the electrolyte and the positive electrode, the composite electrolyte membrane needs to be soaked in a commercial liquid electrolyte (1.0 M $LiPF_6$, EC/DEC (1:1 vol/vol)) for 12 h before use to activate the membrane. The surface electrolyte is then wiped dry with filter paper before the battery is assembled and tested (electrochemical window, ion migration number, and lithium stability experiments are also tested with activated electrolytes). Galvanostatic charge−discharge properties were tested within 2.5–3.9 V for LFP and 2.5−4.2 V for NCM622 using a battery test system (CT2001A, LAND, China).

3. Results and discussion

Fig. 2a shows the surface morphological observation when LATP filling is 10 wt% (CPE-10). As can be seen from the figure, the surface structure of the CPE-10 electrolyte film is compact and smooth, and there is no obvious residue of LATP particles, indicating that LATP particles are well dispersed in the polymer matrix and no aggregation occurs. In addition, it can be seen from the electrolyte optical photos (illustrations in Fig. 2) that CPE-10 is a flexible film with certain transparency, and the section topography of CPE-10

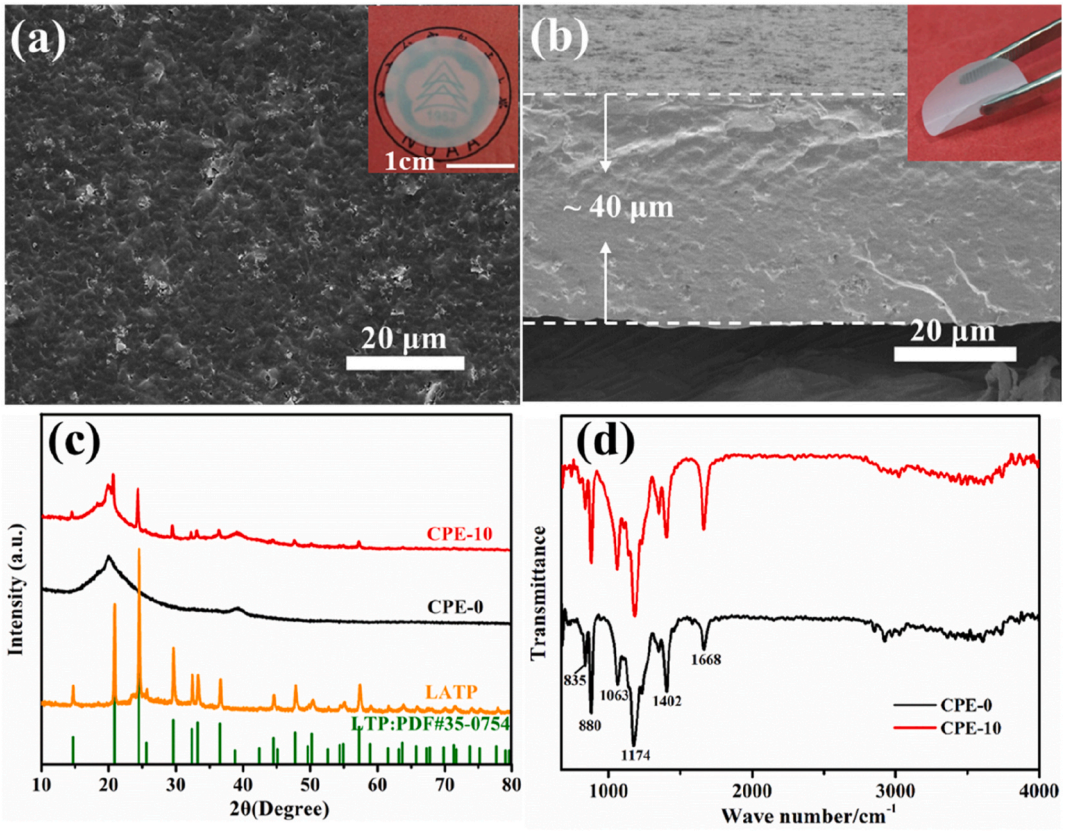

Fig. 2. Microstructure and phase analysis of CPE-10 electrolyte film. SEM images of (a) surface and (b) cross-section of the CPE-10 electrolyte membrane, illustrated as optical photographs of the electrolyte membrane; (c) XRD and (d) FTIR spectra of polyelectrolyte films.

(Fig. 2b) shows that its thickness is about 40 μm, which is in line with the thickness range of polymer electrolyte [33]. The flexibility of the composite electrolyte can effectively alleviate the rigid contact between the electrolyte and the electrode interface and reduce the interface impedance. In addition, the combination of LATP powder and PVDF-HFP polymer avoids direct contact between LATP and lithium-metal, and alleviates the occurrence of interface side reactions to a certain extent.

In addition, to identify the composite phase structural changes of PVDF-HFP, LATP, and CPE-10 films, the XRD diffraction patterns of the three materials are shown in Fig. 2c. Among them, due to the blending with PVDF-HFP, the diffraction peak of LATP on the CPE-10 membrane is relatively weak, indicating that some LATP particles are exposed on the surface of the membrane. In addition, compared with pure PVDF-HFP (CPE-0) electrolyte, the 19–21° diffraction peaks of CPE-10 samples tended to widen, indicating that the addition of LATP particles expanded the amorphous region and reduced the crystallinity of the polymer, thereby improving the electrochemical performance of the polymer electrolyte [34]. Furthermore, the FTIR spectra of the electrolyte membrane was presented in Fig. 2d. The observed peaks at 1668 cm^{-1}, corresponded to the stretching vibration peaks of LiTFSI. The characteristic peaks at 1402 cm^{-1} are assigned to α-phase crystal of PVDF-HFP, while the bands at 880 and 835 cm^{-1} are the amorphous phase. The vibrations bands at 1063, 1174 cm^{-1} corresponded to symmetrical stretching of CF_2, which are shifted after LiTFSI mixing, implying the interaction between PVDF-HFP matrix and LiTFSI [17,35,36]. Before and after the addition of LATP ceramic particles, the FTIR

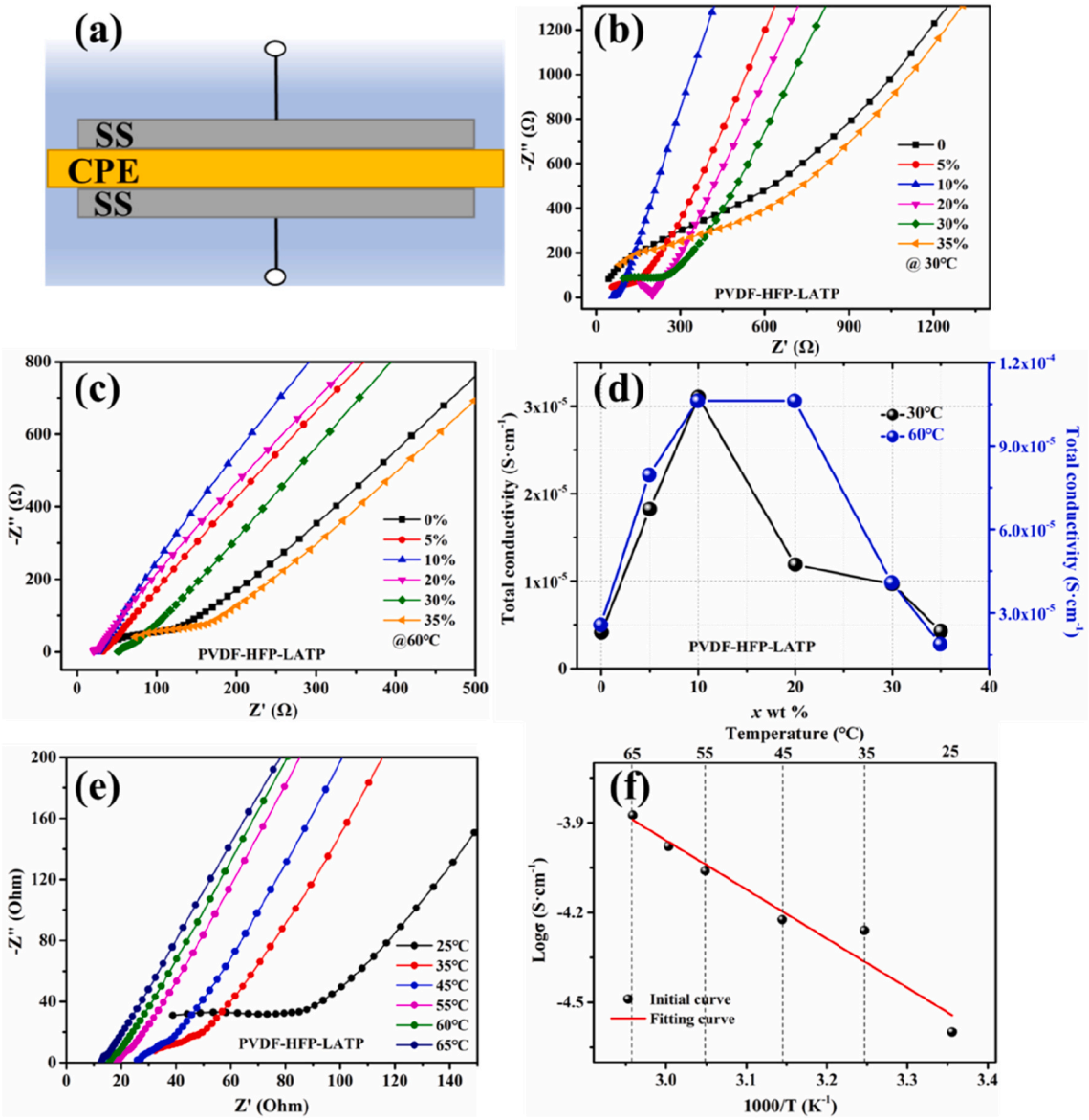

Fig. 3. Analysis of CPE-*x* electrolyte membrane impedance and ionic conductivity. (a) Impedance test battery model, impedance diagram of CPE-x electrolyte film at (b) 30 °C and (c) 60 °C, (d) curve diagram of ionic conductivity with temperature and filling amount, (e) Curve diagram of CPE-10 electrolyte film with temperature and (f) Curve diagram of total ionic conductivity with temperature.

absorption peaks of the electrolyte membrane were similar, and the characteristic peaks did not appear or disappear, indicating that the combination of polymer matrix and LATP ceramic particles was only a physical mixture without any chemical reaction.

Fig. 3a shows the general structure of the battery for testing the impedance performance of the polymer electrolyte. The stainless-steel sheet (SS) serves as the blocking electrode and is clamped on the upper and lower surfaces of the electrolyte to form a "sandwich" structure. Fig. 3b shows the impedance diagram of the modified PVDF-HFP electrolyte at 30 °C with different LATP ceramic filling amounts (0–35 wt%). As can be seen from the figure, all electrolyte samples have a typical electrolyte impedance curve (semi-arc in the high-frequency region and slant in the low-frequency region), and the impedance value (semi-arc diameter) decreases first and then increases as the filling amount increases. When the filling amount is 10 wt% (CPE-10), the minimum impedance value (68 Ω) is obtained. This not only shows that the addition of LATP ceramic powder has a significant effect on the impedance performance, but also shows that the appropriate amount of powder addition is the key to improving the performance.

Fig. 3c shows the corresponding impedance spectra of each group of samples at 60 °C. It can be seen from the figure that the impedance of each component is significantly reduced, and the changing trend of the impedance value with the LATP filling is the same as that at 30 °C. When the filling amount is 10 wt%, the minimum impedance value (25 Ω) is obtained. According to the calculation formula of ionic conductivity, CPE-10 samples can obtain the highest ionic conductivity (3.1×10^{-5} S/cm and 1.06×10^{-4} S/cm) at 30 and 60 °C respectively (Fig. 3d), indicating that when the LATP filling amount is 10 wt%, it is most conducive to the transport of lithium ions in PVDF-HFP polymer electrolyte, to obtain the best performance. The addition of too little powder could not effectively promote the movement of the polymer chain, and lithium ions are mainly transmitted along the polymer matrix, so the impedance performance is not significantly improved. When the powder filling amount is moderate, there are a variety of transmission routes in the composite electrolyte, including polymer matrix, ceramic powder, and interface transmission between powder and polymer, and the transmission routes are interrelated, to ensure the smooth transmission of lithium ions, reduce the transmission impedance and improve the ionic conductivity [37]. When the LATP powder is added in excess, the powder cannot be completely dispersed in the polymer matrix, and even causes a very serious agglomeration phenomenon, which not only may hinder the normal transmission of lithium ions in the powder and the interface, but also may destroy the long chain transmission of lithium ions in the polymer matrix, thereby improving the transmission impedance and reducing the ionic conductivity [38]. Therefore, the content of this chapter mainly focuses on the research of CPE-10 electrolytes, and further explores the transport mechanism of lithium ions in organic-inorganic

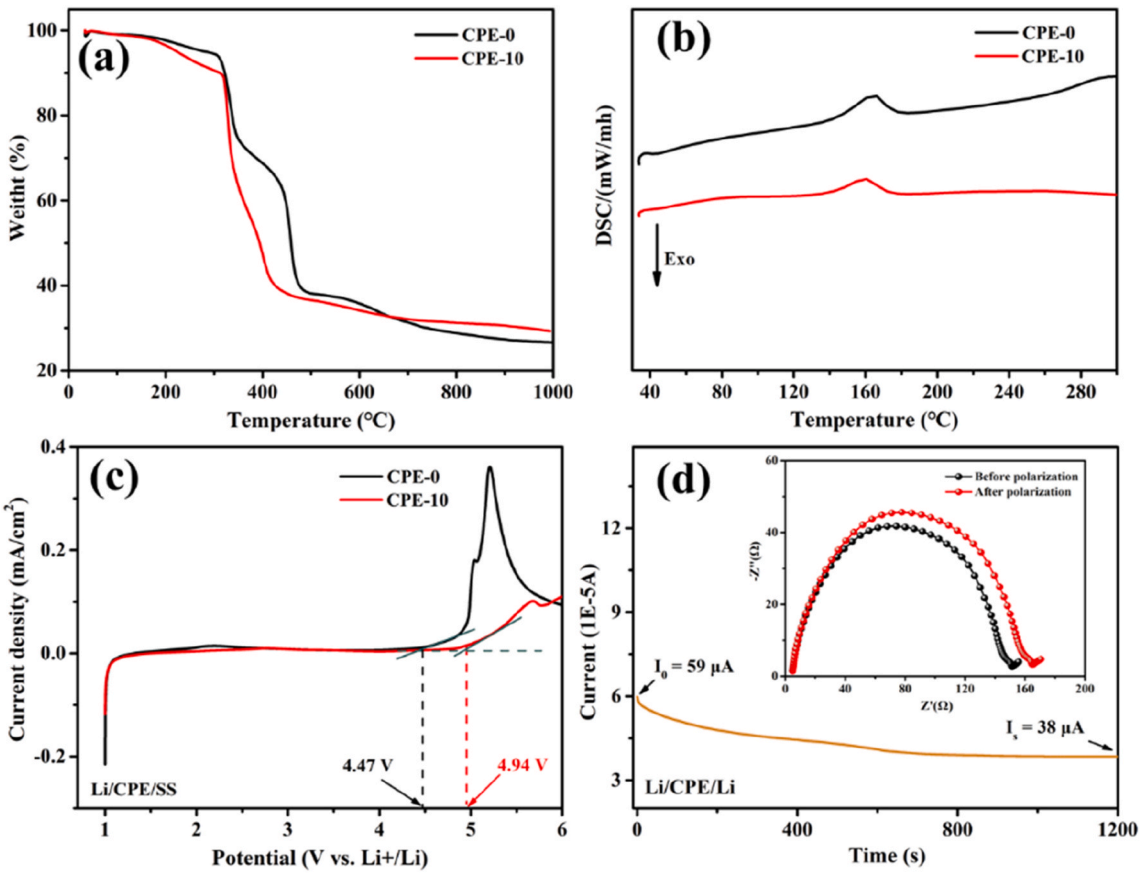

Fig. 4. Analysis of temperature and ion mobility of CPE-*x* thin film electrolyte. (a) TG, (b) DSC, (c) LSV curve and (d) i-t curve of CPE-10 electrolyte membrane.

composite electrolytes.

Fig. 3e shows the impedance diagram of the CPE-10 electrolyte film as a function of temperature. As the temperature continues to increase, the impedance value gradually decreases, which indicates that increasing the temperature is conducive to promoting the transmission of lithium ions in the electrolyte, and thus improving the ionic conductivity. This is mainly because the polymer chain is more likely to move at high temperatures, thus promoting the transfer and transfer of lithium ions, which is also a common phenomenon in solid electrolytes [39]. In addition, according to the total ionic conductivity (σ_t) of the CPE-10 film sample with temperature (Fig. 3f), the activation energy (E_a) of the sample within the test temperature range can be calculated to determine the ease of transport of lithium ions in the electrolyte. As shown in Fig. 3f and calculated by the Arrhenius formula, it can be seen that the activation energy value of the CPE-10 composite electrolyte film is only 0.22eV, which is much smaller than that of many reported polymer electrolytes [39], indicating that lithium ions are easier to move and transfer in the CPE-10 sample. It is also beneficial for the solid electrolyte to maintain high performance over a wide temperature range [40].

Fig. 4a shows the mass of CPE-0 and CPE-10 electrolyte films as a function of temperature. As can be seen from the figure, the thermal degradation of pure PVDF-HFP is about 500 °C. With the addition of LATP powder, the thermal stability of the polymer decreases (410 °C). Compared with CPE-0, CPE-10 film has a larger weight loss before 310 °C, which mainly corresponds to the melting and gradual degradation of the polymer. Among them, the interaction of LATP and polymer matrix increases the amorphous region in the polymer electrolyte, resulting in greater weight loss of the CPE-10 electrolyte before 300 °C [41]. In addition, the CPE-10 film only begins to fully decompose at 310 °C, indicating that it has sufficiently thermal stability to be applied to the research of lithium batteries. Finally, as the test temperature continues to rise, the quality of the two electrolyte membranes tends to remain unchanged. Compared with CPE-0, the CPE-10 membrane has a higher residual mass (corresponding to the residue of LATP powder), which also explains the successful composite of LATP powder and polymer matrix to a certain extent. Fig. 4b shows the DSC curve of the CPE electrolyte film. From the sharp endothermic peaks in the figure, the melting temperature of the electrolyte is reduced after the addition of LATP particles in the PVDF-HFP copolymer. PVDF-HFP (CPE-0) showed a melting peak at 165.8 °C, while LATP nanoparticle-filled polymer (CPE-10) showed a melting peak at 159.5 °C. This is mainly due to the plasticization of LATP particles reducing the crystallinity of PVDF-HFP, and thus reducing the melting point of the polymer.

As shown in Fig. 4c, for the Li/CPE-10/SS battery, the linear sweep voltammetry (LSV) curve is smooth and stable when the test voltage is below 4.94 V. When the voltage is higher than 4.94 V, the curve shows an upward trend, indicating that the electrolyte has an oxidation side reaction, indicating the electrolyte can be used stably under 4.94 V. In contrast, Li/CPE-0/SS batteries undergo a decomposition reaction at 4.47 V, and there is an obvious current fluctuation peak near 2 V, indicating that there is a side reaction between electrolyte and electrode (electrochemical oxidative decomposition of electrolyte). A similar phenomenon has been reported in other polymer electrolytes [42]. However, the specific cause of this phenomenon is not clear, and further structural and mechanism analysis is needed. In conclusion, the above results show that the addition of an appropriate amount of LATP powder can effectively improve the electrochemical window of the polymer electrolyte, which can not only match conventional positive electrodes such as V_2O_5 and $LiFePO_4$, but also improve the use safety of high-voltage positive electrodes ($LiCoO_2$ and NCM ternary, etc.) [15,43].

As shown in Fig. 4d, the lithium-ion migration number (t_{Li+}) of the electrolyte was tested and calculated using the lithium battery structure (Li/CEPE/Li). By polarization, the interface resistance of CPE-10 is increased from 150 Ω to 165 Ω. From the change of current with polarization time, the initial current before polarization is 59 μA, and the current is stable at 38 μA. Therefore, the t_{Li+} value of CPE-10 can be easily calculated as 0.60 according to the Bruce Vincent equation, which is much higher than 0.2 for liquid electrolytes [44] and other PVDF-HFP based polymer electrolytes [2,14,16,17,27,35,45–48] (Table 1). This phenomenon could be related to the interaction between LATP ceramic filler and polymer chain, which relaxed the local chain of polymer and promoted the movement of chain segments [49].

As can be seen from Fig. 5a, the Li/CPE-10/Li battery has a low overpotential (9 mV), while the Li/CPE-0/Li battery exhibited a

Table 1
Performance comparison of the PVDF-HFP based polymer electrolytes.

SPEs	Electrode	Ionic conductivity σ (S/cm)	Li + transference number (t_{Li+})	Electrochemical window (V)	Ref.
ATLLZO/PVDF-HFP	$LiFePO_4$ (2.6–4.2 V)	5.35×10^{-4} (60 °C)	0.37	0.475	[2]
LLZT/PVDF-HFP/IL	$LiFePO_4$ (3.0–3.8 V)	7.63×10^{-4} (100 °C)	0.61	5.3	[14]
LATP/PVDF-HFP	$LiFePO_4$ (2.5–4.0 V)	2.3×10^{-4} (60 °C)	–	–	[16]
LATP/PEG PVDF-HFP	$LiFePO_4$ (2.5–3.6 V)	8.13×10^{-4} (40 °C)	0.58	–	[17]
LLSZO/PVDF-HFP/LiPF6	–	2.94×10^{-3} (35 °C)	4.5	–	[27]
NMP-LE/PVDF-HFP	$LiFePO_4$ (2.5–3.8 V)	7.24×10^{-4} (70 °C)	0.57	5.2	[35]
LLZO/PVDF-HFP	$LiFePO_4$ (2.4–4.0)	3.71×10^{-4} (30 °C)	0.58	4.65	[45]
Lithium magnesium silicate/PVDF-HFP	NCM622 (2.8–4.3 V)	2.56×10^{-4} (25 °C)	0.41	4.8	[46]
LLZTO/PVDF-HFP	$LiFePO_4$ (2.6–3.6 V)	1.04×10^{-4} (45 °C)	0.26	4.7	[47]
g-C_3N_4/PVDF-HFP	/NCM622 (2.8–4.3 V)	1.67×10^{-4} (30 °C)	0.30	4.7	[48]
LATP/PVDF-HFP	**NCM622 (2.5–4.2 V)**	**1.06×10^{-4} (60 °C)**	**0.60**	**4.94V**	**Present work**

higher overpotential (18 mV) at 0.05 mA/cm^2. When the current density increases to 0.1 and 0.2 mA/cm^2, the Li/CPE-0/Li battery has a high overpotential, and becomes very unstable at each voltage platform, indicating that the CPE-0 electrolyte reacts with lithium metal. The introduction of LATP ceramic particles into the PVDF-HFP matrix improves the ion migration number of the electrolyte, so the Li/CPE-10/Li battery has a low overpotential and no obvious voltage fluctuation at 0.1 and 0.2 mA/cm^2. Fig. 5b–d respectively shows the micro-topography of lithium metal surface after Li–Li symmetric test. As can be seen from the figure, the surface of the lithium metal corresponding to the CPE-0 sample produced more granular lithium dendrite particles (Fig. 5b) compared to the surface of the initial lithium metal (Fig. 5c). This is due to the uneven deposition of lithium caused by low CPE-0 lithium ion migration [42]. Compared with CPE-0, the lithium metal surface corresponding to the CPE-10 sample has good smoothness and flatness, and there is no obvious appearance of lithium dendrites (Fig. 5d). Additionally, Fig. 5e shows the galvanostatic cycling tests of CPE-10 thin film cycling for 300 h at current densities of 0.1 mA/cm^2. The cell maintains a low and stable voltage polarization value, indicating that the CPE-10 electrolyte can guarantee the stable reversibility of lithium-ion deportation.

The cyclic performance of the $LiFePO_4$/CPE-10/Li battery at room temperature was tested at a current density of 0.2 C (Fig. 6a). With the increase in the number of cycles, the battery capacity did not decrease significantly, and the charge and discharge curve was relatively smooth in the potential voltage range of 2.5–3.9 V (Fig. 6b), indicating the components in the battery are relatively stable and no side reactions occur [50,51]. After 150 cycles, the coulomb efficiency of the battery reached almost 100%, indicating that the CPE-10 electrolyte membrane could maintain a stable cycle of the battery. Fig. 6c shows the rate performance of the $LiFePO_4$/CPE-10/Li battery. The discharge capacity decreases with the increase of current density, indicating that the capacity loss is limited by the diffusion of lithium ions. The reversible discharge capacity of the battery at 0.1 C is 156 mAh/g, the reversible discharge

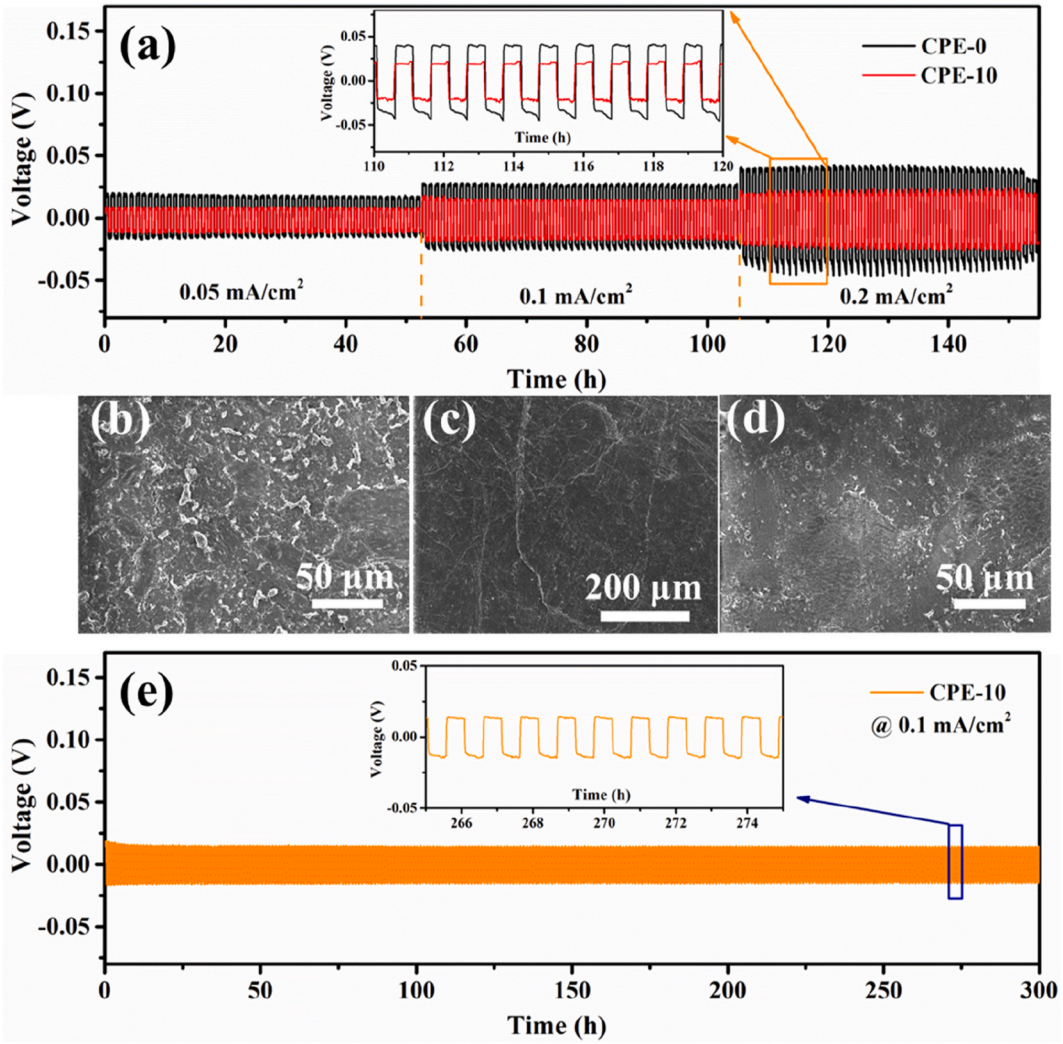

Fig. 5. Performance analysis of CPE-*x* electrolyte on lithium at 60 °C. (a) Lithium stability test of CPE-0 and CPE-10 electrolytes at different current densities; SEM images of the Li electrode surfaces of CPE-0 (b), initial lithium-metal (c), CPE-10 (d) after test at different current densities; and (e) lithium cycling of CPE-10 at 0.1 mA/cm^2 current densities.

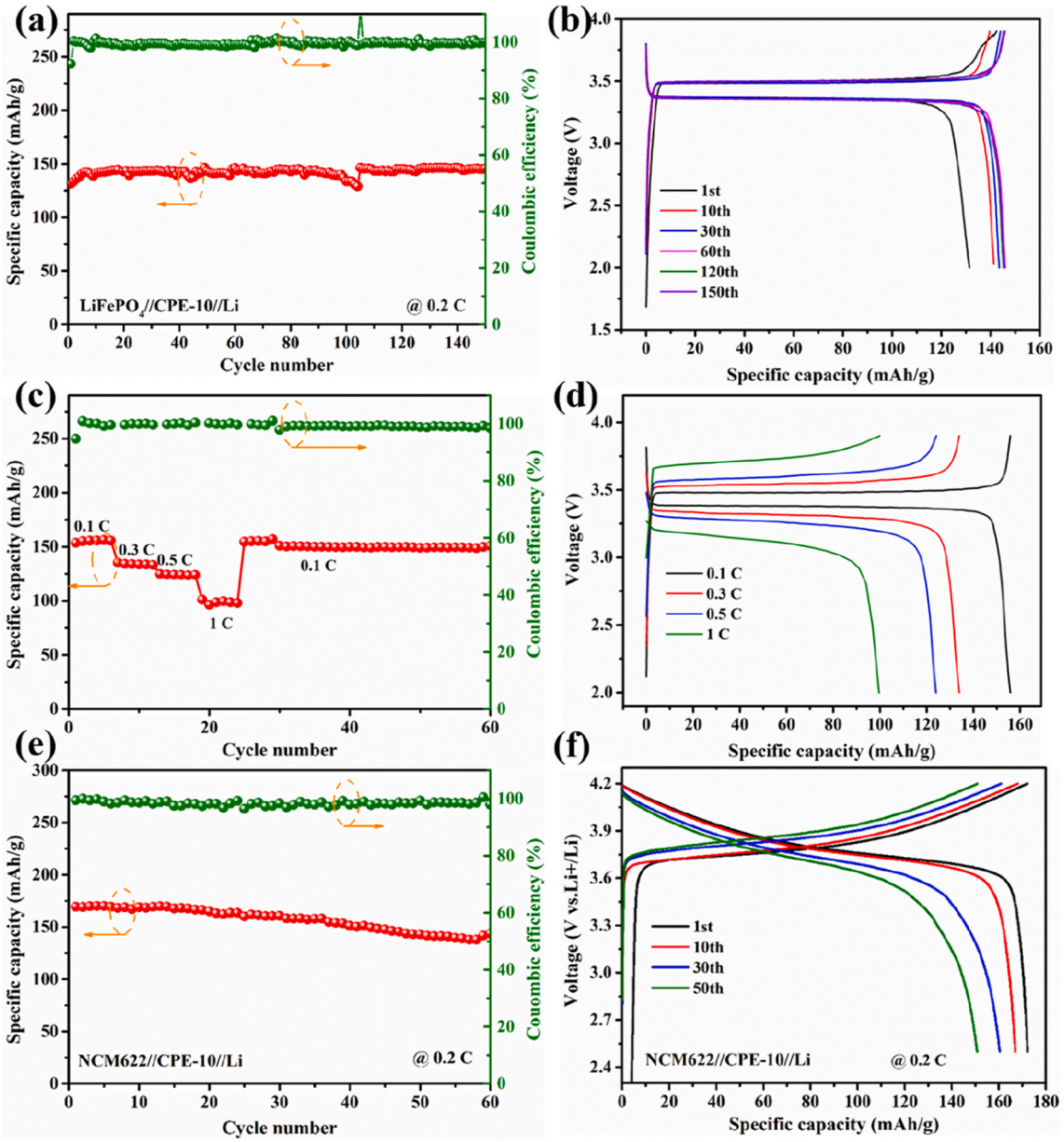

Fig. 6. Analysis of electrochemical performance of the solid-state batteries. Cycling performance (a) and charge and discharge curves (b) under 0.2 C of Li/CPE-10/$LiFePO_4$; Rate performance (c) and initial charge and discharge curves (d) of the Li/CPE-10/$LiFePO_4$ at various current densities at 60 °C. Cycling performance (e) and charge and discharge curves (f) under 0.2 C of Li/CPE-10/NCM622 at 60 °C and 0.2 C.

capacity at 0.5 C is 125 mAh/g, and even at 1 C, the capacity of the battery still reaches 100 mAh/g. When the current density is restored to 0.1C, the battery discharge capacity is restored to 150 mAh/g, showing excellent discharge performance. As shown in Fig. 6d, the $LiFePO_4$/CPE-10/Li battery also has smooth initial charge–discharge curves at different rates within the voltage range.

Basis of the excellent electrochemical performance, high-voltage Li/CPE-10/NCM622 cells were further assembled. Fig. 6e shows the cycle performance of the battery at 0.2 C. The rapid initial lithium-ion homogenization process and construction of lithium-ion transport path provide an initial specific discharge capacity of 171 mAh/g and a first Coulomb efficiency of 96% for Li/CPE-10/NCM622 cells. After 50 charge–discharge cycles, the Li/CPE-10/NCM622 battery shows the highest specific discharge capacity of 152 mAh/g and Coulomb efficiency of nearly 100% with smooth charge–discharge curves (Fig. 6f), indicating that CPE-10 can achieve highly reversible lithium-ion disembedding behavior in the potential voltage range of 3.0–4.2 V.

4. Conclusion

In summary, we have prepared a composite electrolyte film (CPE-10) with a uniform distribution of inorganic LATP and PVDF-HFP polymers by tape-casting method, and assembled Li/CPE-10/$LiFePO_4$ and Li/CPE-10/NCM622 solid-state lithium batteries. The CPE-10 composite electrolyte membrane has higher ionic conductivity (1.06 × 10-4 S/cm) and higher Li^+ transference number (0.60). The addition of rigid LATP ceramic particles effectively improves the electrochemical window of the electrolyte (4.94 V), which is expected to solve the safety problem of high-voltage lithium metal batteries. In addition, the CPE-10 electrolyte not only has good temperature stability, but also has excellent stability against lithium: at 0.1 mA/cm^2 current density, it can be stably cycled for 300 h with effective lithium dendrite inhibition. Li/CPE-10/$LiFePO_4$ batteries also obtain excellent cycle performance: at 0.2C current density, the discharge capacity remains at 150 mAh/g after 150 cycles. Moreover, the high-voltage Li/CPE-10/NCM622 cells showed the highest specific discharge capacity of 152 mAh/g and Coulomb efficiency of nearly 100% after 50 cycles. In short, the composite design of the CPE-10 membrane could have great application potential in the field of lithium metal batteries.

Data availability statement

Data will be made available on request.

Additional information

No additional information is available for this paper.

CRediT authorship contribution statement

Zhongran Yao: Writing – review & editing, Writing – original draft, Formal analysis, Data curation, Conceptualization. **Fen Qi:** Writing – review & editing, Writing – original draft, Data curation, Conceptualization. **Lin Ye:** Data curation, Conceptualization. **Qiang Sun:** Software, Funding acquisition, Formal analysis. **Xiaoyong Gu:** Conceptualization. **Xiaowei Yang:** Conceptualization. **Kongjun Zhu:** Conceptualization.

Declaration of competing interest

The authors declare that they have no known competing financial interests or personal relationships that could have appeared to influence the work reported in this paper.

Acknowledgements

This work was supported by the Natural Science Research of Jiangsu Higher Education Institutions of China (No. 23KJB430038), the Research and Innovation Team Building Project of Wuxi Institute of Technology (ZKTD04); the Natural Science Research Project of Wuxi Institute of Technology (BT2023-06).

References

[1] C. Park, S. Na, H.G. Park, K. Park, Synergistic effect of Calcination and sintering on the reduction of Grain Boundary resistance of LATP solid electrolyte, ACS Appl. Mater. Interfaces 15 (22) (2023) 26985–26992.
[2] J. Zou, X. Gao, X. Zhou, J. Yang, J. Tang, H. Kou, R. Chang, Y. Zhang, Al and Ta co-doped LLZO as active filler with enhanced Li^+ conductivity for PVDF-HFP composite solid-state electrolyte, Nanotechnology 34 (15) (2023) 155402.
[3] H. Yang, M. Jing, L. Wang, H. Xu, X. Yan, X. He, PDOL-based solid electrolyte toward Practical application: Opportunities and challenges, Nano-Micro Lett. 16 (1) (2024).
[4] A.G. Sabato, M. Nuñez Eroles, S. Anelli, C.D. Sierra, J.C. Gonzalez-Rosillo, M. Torrell, A. Pesce, G. Accardo, M. Casas-Cabanas, P. López-Aranguren, A. Morata, A. Tarancón, 3D printing of self-supported solid electrolytes made of glass-derived $Li_{1.5}Al_{0.5}Ge_{1.5}P_3O_{12}$ for all-solid-state lithium-metal batteries, J. Mater. Chem. A 11 (25) (2023) 13677–13686.
[5] Z. Ren, J. Li, M. Cai, R. Yin, J. Liang, Q. Zhang, C. He, X. Jiang, X. Ren, Anin situformed copolymer electrolyte with high ionic conductivity and high lithium-ion transference number for dendrite-free solid-state lithium metal batteries, J. Mater. Chem. A 11 (4) (2023) 1966–1977.
[6] L. Du, B. Zhang, X. Wang, C. Dong, L. Mai, L. Xu, 3D frameworks in composite polymer Electrolytes: synthesis, Mechanisms, and applications, Chem. Eng. J. (Lausanne) 451 (2023) 138787.
[7] H. Chen, X. Cao, M. Huang, X. Ren, Y. Zhao, L. Yu, Y. Liu, L. Zhong, Y. Qiu, In-situ interfacial passivation and self-adaptability synergistically stabilizing all-solid-state lithium metal batteries, J. Energy Chem. 88 (2024) 282–292.
[8] W.-w. Shao, J.-x. Li, L. Zhong, H.-f. Wu, M.-q. Liu, Y. Mei, L.-p. Zhou, H.-x. Liu, M.-x. Jing, A high ion conductive solid electrolyte film and interface stabilization strategy for solid-state Li-S battery, Colloid. Surface. 679 (2023) 132593.
[9] C.-H. Tsao, C.-Y. Wang, E. Trevisanello, F.H. Richter, D. Kuo, J. Janek, C.-H. Chang, H. Teng, P.-L. Kuo, Polyethylene glycol dimethyl ether-plasticized poly (vinylidene difluoride)-based polymer electrolytes inhibit dendrite growth and enable stable cycling for lithium-metal batteries, ACS Appl. Energy Mater. 6 (2023) 5662–5670.
[10] Z. Yao, K. Zhu, X. Li, J. Zhang, J. Chen, J. Wang, K. Yan, J. Liu, 3D poly(vinylidene fluoride–hexafluoropropylen) nanofiber-reinforced PEO-based composite polymer electrolyte for high-voltage lithium metal batteries, Electrochim. Acta 404 (2022) 139769.
[11] M. Cai, C. Zheng, J. Li, C. Shi, R. Yin, Z. Ren, J. Hu, Y. Li, C. He, Q. Zhang, X. Ren, Revealing the role of hydrogen bond coupling structure for enhanced performance of the solid-state electrolyte, J. Colloid Interface Sci. 652 (2023) 529–539.
[12] Y. Cui, J. Wan, Y. Ye, K. Liu, L.Y. Chou, Y. Cui, A. Fireproof, Lightweight, polymer-polymer solid-state electrolyte for safe lithium batteries, Nano Lett. 20 (3) (2020) 1686–1692.

[13] Yusong Zhu, Shiying Xiao, Yi Shi, Yaqiong Yang, Yuyang Hou, Y. Wu, A composite gel polymer electrolyte with high performance based on poly(vinylidene fluoride) and polyborate for lithium ion batteries, Adv. Energy Mater. 4 (2014) 1300647.
[14] W. Zhang, J. Nie, F. Li, Z.L. Wang, C. Sun, A durable and safe solid-state lithium battery with a hybrid electrolyte membrane, Nano Energy 45 (2018) 413–419.
[15] C.-C. Yang, Z.-Y. Lian, S.J. Lin, J.-Y. Shih, W.-H. Chen, Preparation and application of PVDF-HFP composite polymer electrolytes in $LiNi_{0.5}Co_{0.2}Mn_{0.3}O2$ lithium-polymer batteries, Electrochim. Acta 134 (2014) 258–265.
[16] Y. Li, H. Wang, Composite solid electrolytes with NASICON-type LATP and PVdF–HFP for solid-state lithium batteries, Ind. Eng. Chem. Res. 60 (3) (2021) 1494–1500.
[17] T. Zhao, Q. Gai, X. Deng, J. Ma, H. Gao, A new type of LATP doped PVDF-HFP based electrolyte membrane with flame retardancy and long cycle stability for solid state batteries, J. Energy Storage 73 (2023) 108576.
[18] Y.T. Chen, Y.C. Chuang, J.H. Su, H.C. Yu, Y.W. Chen-Yang, High discharge capacity solid composite polymer electrolyte lithium battery, J. Power Sources 196 (5) (2011) 2802–2809.
[19] S. Ahmad, T.K. Saxena, S.A. Ahmad, S.A. Agnihotry, The effect of nanosized TiO_2 addition on poly(methylmethacrylate) based polymer electrolytes - ScienceDirect, J. Power Sources 159 (1) (2006) 205–209.
[20] A.K. Solarajan, V. Murugadoss, S. Angaiah, Dimensional stability and electrochemical behaviour of ZrO2 incorporated electrospun PVdF-HFP based nanocomposite polymer membrane electrolyte for Li-ion capacitors, Sci. Rep. 7 (2017) 45390.
[21] S. Jayanthi, K. Kulasekarapandian, A. Arulsankar, K. Sankaranarayanan, B. Sundaresan, Influence of nano-sized TiO_2 on the structural, electrical, and morphological properties of polymer-blend electrolytes PEO-PVC-$LiClO_4$, J. Compos. Mater. 12 (9) (2011) 1695–1700.
[22] O. Sheng, C. Jin, J. Luo, H. Yuan, C. Fang, H. Huang, Y. Gan, J. Zhang, Y. Xia, C. Liang, Ionic conductivity promotion of polymer electrolyte with ionic liquid grafted oxides for all-solid-state lithium–sulfur batteries, J. Mater. Chem. A 5 (2017) 12934–12942.
[23] J. Zhang, N. Zhao, M. Zhang, Y. Li, P.K. Chu, X. Guo, Z. Di, X. Wang, H. Li, Flexible and ion-conducting membrane electrolytes for solid-state lithium batteries: dispersion of garnet nanoparticles in insulating polyethylene oxide, Nano Energy 28 (2016) 447–454.
[24] W. Xiao, J. Wang, L. Fan, J. Zhang, X. Li, Recent advances in $Li_{1+x}Al_xTi_{2-x}(PO_4)_3$ solid-state electrolyte for safe lithium batteries, Energy Storage Mater. 19 (2019) 379–400.
[25] M. Kotobuki, M. Koishi, Preparation of $Li_{1.3}Al_{0.3}Ti_{1.7}(PO_4)_3$ solid electrolyte via a sol-gel method using various Ti sources, J Asian Ceram Soc 8 (3) (2020) 891–897.
[26] J. Liang, J. Luo, Q. Sun, X. Yang, R. Li, X. Sun, Recent progress on solid-state hybrid electrolytes for solid-state lithium batteries, Energy Storage Mater. 21 (2019) 308–334.
[27] D.K. Maurya, B. Balan, V. Murugadoss, C. Yan, S. Angaiah, A fast Li-ion conducting $Li_{7.1}La_3Sr_{0.05}Zr_{1.95}O_{12}$ embedded electrospun PVDF-HFP nanohybrid membrane electrolyte for all-solid-state Li-ion capacitors, Mater. Today Commun. 25 (2020) 101497.
[28] I. Stenina, A. Pyrkova, A. Yaroslavtsev, NASICON-type $Li_{1+x}Al_xZr_yTi_{2-x-y}(PO_4)_3$ solid electrolytes: effect of Al, Zr Co-doping and synthesis method, Batteries 9 (1) (2023) 59.
[29] L. Hallopeau, D. Bregiroux, G. Rousse, D. Portehault, P. Stevens, G. Toussaint, C. Laberty-Robert, Microwave-assisted reactive sintering and lithium ion conductivity of $Li_{1.3}Al_{0.3}Ti_{1.7}(PO_4)_3$ solid electrolyte, J. Power Sources 378 (2018) 48–52.
[30] K. Zou, Z. Cai, X. Ke, K. Wang, X. Tan, D. Luo, F. Huang, C. Wang, J. Cheng, R. Xiao, Electrochemical properties of LATP ceramic electrolyte doped with $LiBiO_3$ sintering additive and its derived sandwich structure composite solid electrolyte, Ionics 29 (7) (2023) 2665–2678.
[31] Y.-J. Wang, Y. Pan, D. Kim, Conductivity studies on ceramic $Li_{1.3}Al_{0.3}Ti_{1.7}(PO_4)_3$-filled PEO-based solid composite polymer electrolytes, J. Power Sources 159 (1) (2006) 690–701.
[32] Z. Yao, K. Zhu, J. Zhang, X. Li, J. Chen, J. Wang, K. Yan, J. Liu, Co-precipitation synthesis and electrochemical properties of NASICON-type $Li_{1.3}Al_{0.3}Ti_{1.7}(PO_4)_3$ solid electrolytes, J. Mater. Sci. Mater. Electron. 32 (2021) 24834–24844.
[33] X. Yang, K.R. Adair, X. Gao, X. Sun, Recent advances and perspectives on thin electrolytes for high-energy-density solid-state lithium batteries, Energy Environ. Sci. 14 (2021) 643–671.
[34] Y. Xia, X. Wang, X. Xia, R. Xu, S. Zhang, J. Wu, Y. Liang, C. Gu, J. Tu, A newly designed composite gel polymer electrolyte based on poly(vinylidene fluoride-hexafluoropropylene) (PVDF-HFP) for enhanced solid-state lithium-sulfur batteries, Chemistry 23 (60) (2017) 15203–15209.
[35] J. Jie, Y. Liu, L. Cong, B. Zhang, W. Lu, X. Zhang, J. Liu, H. Xie, L. Sun, High-performance PVDF-HFP based gel polymer electrolyte with a safe solvent in Li metal polymer battery, J. Energy Chem. 49 (2020) 80–88.
[36] W. Liu, C. Yi, L. Li, S. Liu, Q. Gui, D. Ba, Y. Li, D. Peng, J. Liu, Designing polymer-in-salt electrolyte and fully infiltrated 3D electrode for integrated solid-state lithium batteries, Angew. Chem. Int. Ed. 60 (23) (2021) 12931–12940.
[37] J. Zheng, Y.-Y. Hu, New insights into the compositional dependence of Li-ion transport in polymer-ceramic composite electrolytes, ACS Appl. Mater. Interfaces 10 (4) (2018) 4113–4120.
[38] D. Zhang, X. Xu, Y. Qin, S. Ji, Y. Huo, Z. Wang, Z. Liu, J. Shen, J. Liu, Recent progress in organic-inorganic composite solid electrolytes for all-solid-state lithium batteries, Chemistry 26 (8) (2020) 1720–1736.
[39] X. Zhang, T. Liu, S. Zhang, X. Huang, B. Xu, Y. Lin, B. Xu, L. Li, C.W. Nan, Y. Shen, Synergistic coupling between $Li_{6.75}La_3Zr_{1.75}Ta_{0.25}O_{12}$ and poly(vinylidene fluoride) induces high ionic conductivity, mechanical strength, and thermal stability of solid composite electrolytes, J. Am. Chem. Soc. 139 (39) (2017) 13779–13785.
[40] J.-F. Wu, W.K. Pang, V.K. Peterson, L. Wei, X. Guo, Garnet-type fast Li-ion conductors with high ionic conductivities for all-solid-state batteries, ACS Appl. Mater. Interfaces 9 (14) (2017) 12461–12468.
[41] W.H. Hou, C.Y. Chen, C.C. Wang, Y.H. Huang, The effect of different lithium salts on conductivity of comb-like polymer electrolyte with chelating functional group, Electrochim. Acta 48 (6) (2003) 679–690.
[42] Z. Zhao, Y. Zhang, S. Li, S. Wang, Y. Li, H. Mi, L. Sun, X. Ren, P. Zhang, A lithium carboxylate grafted dendrite-free polymer electrolyte for an all-solid-state lithium-ion battery, J. Mater. Chem. A 7 (2019) 25818–25823.
[43] W. Zhou, Z. Wang, Y. Pu, Y. Li, S. Xin, X. Li, J. Chen, J.B. Goodenough, Double-layer polymer electrolyte for high-voltage all-solid-state rechargeable batteries, Adv Mater 31 (4) (2019) e1805574.
[44] M. Liu, D. Zhou, Y.B. He, Y. Fu, X. Qin, C. Miao, H. Du, B. Li, Q.H. Yang, Z. Lin, Novel gel polymer electrolyte for high-performance lithium–sulfur batteries, Nano Energy (2016) 278–289.
[45] Y.F. Liang, S.J. Deng, Y. Xia, X.L. Wang, X.H. Xia, J.B. Wu, C.D. Gu, J.P. Tu, A superior composite gel polymer electrolyte of $Li_7La_3Zr_2O_{12}$-poly (vinylidene fluoride-hexafluoropropylene) (PVDF-HFP) for rechargeable solid-state lithium ion batteries, Mater. Res. Bull. 302 (2018) 412–417.
[46] J. Li, W. Zheng, L. Zhu, H. Zhou, K. Zhang, Incorporating lithium magnesium silicate into PVDF-HFP based solid electrolyte to achieve advanced solid-state lithium-ion batteries, J Alloy Compound 960 (2023) 170640.
[47] P. Yadav, M.S. Hosen, P.K. Dammala, P. Ivanchenko, J. Van Mierlo, M. Berecibar, Development of composite solid polymer electrolyte for solid-state lithium battery: incorporating LLZTO in PVDF-HFP/LiTFSI, Solid State Ionics 399 (2023) 116308.
[48] J. Li, L. Zhu, H. Xie, W. Zheng, K. Zhang, Graphitic carbon nitride assisted PVDF-HFP based solid electrolyte to realize high performance solid-state lithium metal batteries, Colloid. Surface. 657 (2023) 130520.
[49] H.T. Le, D.T. Ngo, R.S. Kalubarme, G. Cao, C.N. Park, Composite gel polymer electrolyte based on poly(vinylidene fluoride-hexafluoropropylene) (PVDF-HFP) with modified aluminum-doped lithium lanthanum titanate (A-LLTO) for high-performance lithium rechargeable batteries, ACS Appl. Mater. Interfaces 8 (32) (2016) 20710–20719.
[50] M. Wu, D. Liu, D. Qu, Z. Xie, J. Li, J. Lei, H. Tang, 3D coral-like LLZO/PVDF composite electrolytes with enhanced ionic conductivity and mechanical flexibility for solid-state lithium batteries, ACS Appl. Mater. Interfaces 12 (47) (2020) 52652–52659.
[51] P. Zhai, N. Peng, Z. Sun, W. Wu, W. Kou, G. Cui, K. Zhao, J. Wang, Thin laminar composite solid electrolyte with high ionic conductivity and mechanical strength towards advanced all-solid-state lithium–sulfur battery, J. Mater. Chem. A 8 (44) (2020) 23344–23353.